Manipulation of Athermal Nuclei in Aqueous Poly(ethylene oxide) by Scanning Activity Gravimetric Analysis

Adam P. Olsen, Richard C. Flagan,* and Julia A. Kornfield*

Division of Chemistry and Chemical Engineering, California Institute of Technology, Pasadena, California 91125

Received July 4, 2006

ABSTRACT: We show that polymer solutions exhibit memory effects as they undergo repeated dissolution (deliquescence) and crystallization (efflorescence) transitions, similar to those previously observed in polymer melts. These memory effects have been probed using scanning activity gravimetric analysis (SAGA) on aqueous poly(ethylene oxide). SAGA is a new method that enables manipulation of the thermodynamic state of a polymer/solvent system under isothermal conditions. The measurements have been performed on individual micron-sized (∼10 ng) polymer particles that are levitated electrostatically and subjected to programmed changes in the activity of solvent vapor. The particle mass rapidly changes due to sorption or evaporation of solvent in response to changes in vapor activity, providing insights into the changing state of the polymer/solvent system. Repeated cycling of solvent activity within a levitated particle reveals systematic shifts up and down in the deliquescence and efflorescence activities depending upon the extreme activities reached. Melt memory effects have previously been attributed to remnants of lamellar crystals that persist beyond the nominal melting temperature. The present observations suggest that the thickness of these remnants evolves in solution, changing the supersaturation at which they may serve as athermal nuclei. An extension to the classical thermodynamic model of lamellae that includes a reduced interfacial tension at the perimeter of the high energy fold surface predicts the existence of a metastable radius that allows remnants to slowly increase or decrease in thickness under certain conditions, thereby rationalizing the ability to manipulate efflorescence behavior. We also present an analysis that suggests that SAGA can be extended to other polymer/solvent systems with the appropriate choice of temperature.

Introduction

Polymers crystallize to form metastable chain-folded platelets called lamellae, rather than extended-chain crystals, because of kinetic limitations.[1] Lamellae have very large surface-to-volume ratios and, therefore, must grow far from equilibrium, where the bulk free energy gain is sufficient to overcome the cost of the high energy fold surface. Since crystallization is an activated process, lamellae emerge with a thickness that is greater than the marginally stable thickness at the growth conditions, so hysteresis is always observed between crystallization and dissolution or melting. After primary crystallization, crystallinity often increases further over long times as a result of sluggish secondary processes such as interlamellar crystallization[2] and thickening of preexisting lamellae.[3,4]

Memory effects in semicrystalline polymers have been documented for a variety of systems in which the rate of crystallization depends on the temperature and duration of a prior melting step.[5−13] This phenomenon is usually attributed to small remnants of the crystalline phase that persist for long times above the apparent melting temperature and then serve as athermal nuclei[14] upon cooling. Although many believe that remnants survive exclusively because of sluggish kinetics,[9−13,15] thermodynamic considerations may also play an important role.[16−18]

We previously introduced scanning activity gravimetric analysis (SAGA) as a novel technique for investigating polymer crystallization from concentrated polymer solution under isothermal conditions.[19] This paper reports memory effects observed by SAGA in aqueous poly(ethylene oxide) (PEO). The present results suggest that small remnants of lamellae persist beyond the apparent dissolution point. At water activities above the value that dissolves all detectable lamellae, the remnants gradually evolve toward increasing or decreasing thickness in response to certain processing protocols, as indicated by a shift in the conditions at which they catalyze crystal growth when the concentration of the polymer solution is subsequently increased. A simple model describing the free energy of a lamellar crystal based on insights of Janeschitz-Kriegl[16−18] captures the metastability of lamellar remnants and their evolution in thickness. The qualitative successes of the model lend support to the thermodynamic rationalization of memory effects in semicrystalline polymers.

* Corresponding authors. E-mail: flagan@caltech.edu, jak@cheme.caltech.edu.

Experimental Section

An automated single particle electrostatic levitation system, described in detail elsewhere,[20] was used to perform scanning activity gravimetric analysis (SAGA) on PEO (Sigma Aldrich Co., M_w = 100 000 g/mol), scanning the activity of water. A three-dimensional electrostatic field generated by a cage of electrodes (Figure 1a) suspends a micron-sized charged particle against gravitational, aerodynamic, and Brownian forces; the dc balancing voltage (V_b) applied across the disk electrodes shown in Figure 1a is proportional to mass. Automated position control maintains the particle within a finite view volume defined by an illuminating laser beam. The balancing voltage is continuously recorded as the sorbed water content equilibrates with the humid atmosphere during an experiment. The relative mass (m/m_0) is calculated by normalizing the instantaneous balancing voltage by the balancing voltage in the dry state, i.e., $m/m_0 = V_b/V_{b,dry}$. The relative humidity, or, equivalently, the water activity a_w, and temperature of a nitrogen atmosphere surrounding the particle are strictly regulated by an environmental control module. The apparatus can be programmed to impose any desired water activity history; the experiments described below use simple constant rate scans and steps.

Dissolution and crystallization are directly observed through changes in sorbed water content and optical properties. When all crystallites dissolve, the sample becomes a spherical droplet of

10.1021/ma0614949 CCC: $33.50
Published on Web 11/07/2006

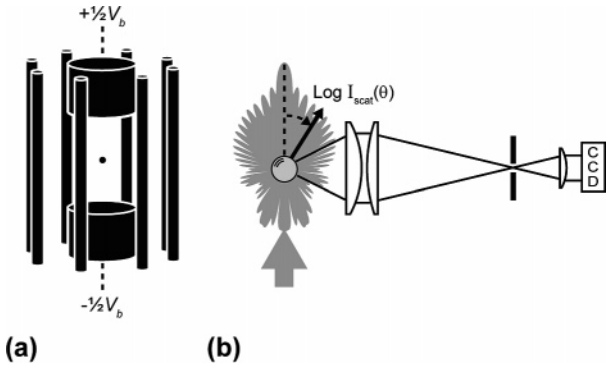

Figure 1. (a) A single charged particle is levitated using electrostatic forces that can be dynamically adjusted using an electrode cage to hold the particle at the geometric center in the environmental control chamber that imposes a programmed history of conditions of water activity (relative humidity) and temperature. A laser beam (532 nm, 25 mW) is incident on the particle, and the scattered intensity is observed over a selected angular range. (b) View down the central axis of the electrode cage illustrates the angular range (78°−102° relative to the incident laser beam) over which the scattered intensity is monitored. Radiation is focused through an aperture and collimated onto a CCD detector. The schematic shows the Mie pattern of scattered light intensity calculated for a 5 μm droplet illustrated as a logarithmic polar plot of the intensity as a function of angle.

polymer solution. A micron-sized optically homogeneous sphere, such as a small solution droplet, produces a well-defined angular scattering pattern when illuminated by coherent light. This Mie pattern[21] exhibits a series of peaks and valleys in scattered intensity (Figure 1b). The angular frequency of the pattern increases with diameter, providing a measure of the absolute size of the solution droplet. In contrast, an aspherical particle, or one with internal heterogeneity, produces an irregular light scattering pattern. The Mie pattern is, therefore, lost upon formation of a crystallite in a droplet of supersaturated solution.

Gravimetric data presented below were recorded during experiments using three different particles of PEO taken from the same batch of material, distinguished as PEO-1, PEO-2, and PEO-3. Each particle has a mass of several nanograms, so it is possible that variations in composition that might not be evident macroscopically could cause differences among different 10 ng samples of a given material. Therefore, it is significant that the results on these three distinct particles accord well with each other and with measurements made on a number of other particles of the same PEO.

Results

The response of PEO-1 to varying water activity (a_w) was recorded continuously for 70 h (Figure 2). The activity of water vapor surrounding the particle was programmed to alternately decrease and increase at a constant scan rate of 0.05 h^{-1} at 20.25 ± 0.05 °C. Each cycle is assigned a letter, and the increasing half of the scan is indicated by a prime (e.g., A/A′). The minimum value of each cycle was held constant at $a_{w,min} = 0.72$. The peak value was $a_{w,max} = 0.92$ for the first set of scans (A′−F′) and increased to $a_{w,max} = 0.95$ for two subsequent scans (G′ and H′).

As a_w increased during each primed scan (e.g., A′), the PEO particle first sorbed little water vapor and exhibited uncorrelated light scattering since the sample remained highly crystalline (Figure 3). At sufficiently high a_w, however, the least stable lamellae in the crystallite population began to dissolve, and the water sorption increased significantly with increasing a_w. Further increase in a_w eventually dissolved the entire population, signified by a sharp decrease in the rate of water sorption and the emergence of Mie scattering; the semicrystalline PEO particle had "deliquesced" and become a spherical aqueous solution droplet. The conversion between balancing voltage and mass is established using the fully solvated state in which the density is approximately that of water and the volume is computed from the scattering pattern (Figure 3, top) using Mie theory (the droplet of polymer solution is an optically uniform sphere with refractive index between that of water and PEO, n ≈ 1.40). Applying the resulting conversion factor to the balancing voltage required for PEO-1 in the dry state reveals its mass is 11 ± 1 ng (corresponding to a dry particle diameter of ∼26 μm).

Reducing a_w during scan B decreased the water content to create an increasingly concentrated solution. As the droplet evaporated water, the reduction in volume was accompanied by a decrease in the number of fringes observed in the angular light scattering pattern (Figure 3, top). As a_w decreased, the solution eventually became sufficiently supersaturated that nucleation occurred and crystalline lamellae propagated throughout the particle, driving the evaporation of water and disrupting the light scattering pattern during a process known as "efflorescence".

A parametric plot of the recorded mass as a function of a_w clearly illustrates hysteresis between dissolution and crystallization (Figure 4a): the activity of water required to dissolve the crystallites during the upward scan was significantly greater than the activity of water at which nucleation and growth of crystallites occurred during the downward scan. Since the solution−vapor isotherm represents a state of zero (undetectable) crystallinity, it is useful to transform the relative mass into an index (I_c) that increases from 0 in the fully dissolved solution to 1 as crystallinity increases:[19]

$$I_c(a_w) = \frac{m_{sol}(a_w) - m(a_w)}{m_{sol}(a_w) - m_0} \quad (1)$$

where m_0 is the mass of the dry PEO particle, $m(a_w)$ is the actual

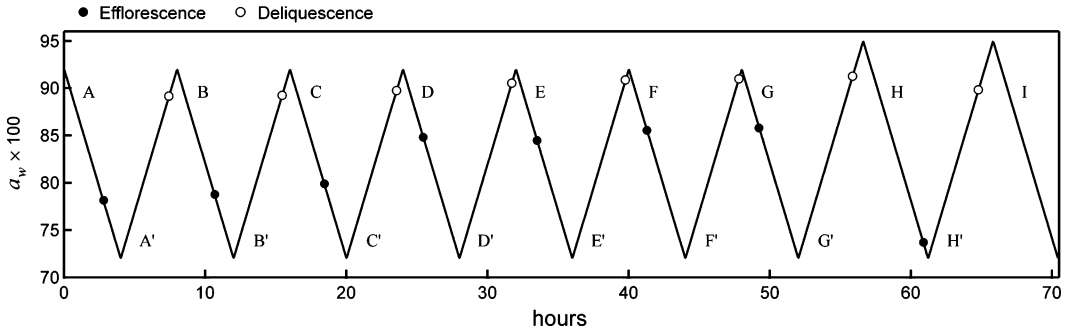

Figure 2. Response of PEO-1 to repeated continuous triangular scans in water activity between 0.72 and 0.92 (A−G) and between 0.72 and 0.95 (G′−I) at 0.05 h^{-1} under isothermal conditions ($T = 20.25 \pm 0.05$ °C). During each downward scan, the time at which a dramatic decrease in mass due to crystallization (efflorescence transition) occurred is indicated by a filled circle (●). During each upward scan, the time at which an abrupt increase in mass due to dissolution (deliquescence transition) occurred is indicated by an open circle (○).

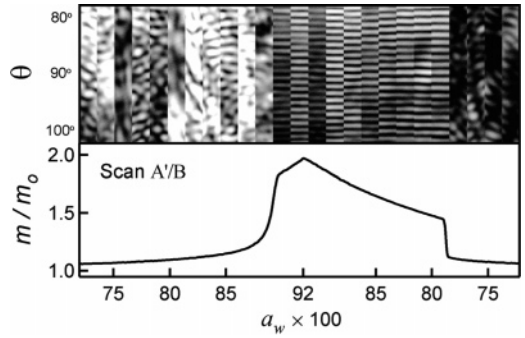

Figure 3. Light scattering pattern (captured at 20 min intervals) and normalized particle mass m/m_0 (recorded at 20 s intervals) as functions of water activity a_w during upward scan A′ and downward scan B of Figure 2. The a_w axis also corresponds to a linear increase in time (8 h total). The particle begins in a semicrystalline solid state with a small amount of sorbed water. When a_w reaches ~0.9, the mass increases strongly and the image of the angular light scattering indicates that an optically homogeneous spherical solution droplet forms. From this transition onward to the peak $a_{w,max}$ and down to $a_w \approx 0.8$, the water content of the sample follows the solution isotherm for the PEO/water system. The transition from semicrystalline sorption behavior to solution sorption behavior is the deliquescence transition. The reverse transition from the solution to the semicrystalline state, known as efflorescence, is marked by the disappearance of the Mie pattern and an abrupt decrease in mass.

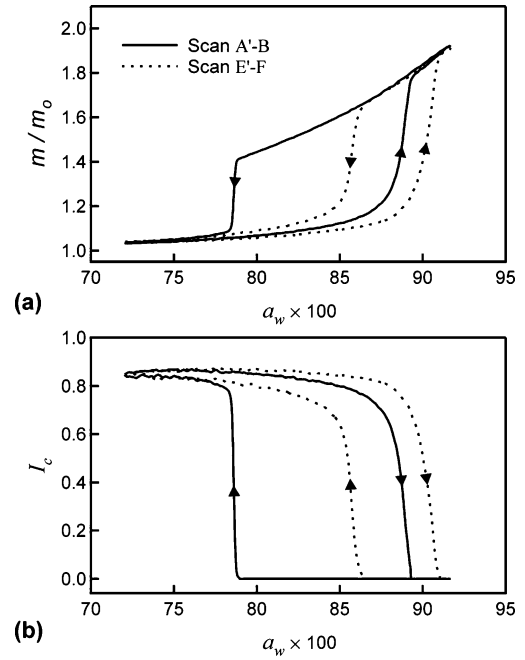

Figure 4. (a) m/m_0 vs a_w and (b) I_c vs a_w for scans A′/B (solid trace) and E′/F (dashed trace) of Figure 2.

mass of the PEO particle at a given water activity, and $m_{sol}(a_w)$ is the mass of the fully dissolved PEO solution droplet at a given water activity.

Since a given efflorescence or deliquescence event occurs over a range in activity (Figures 3 and 4), the nominal activity for each transition ($a_{w,e}$ or $a_{w,d}$) is defined as the activity at which the maximum rate of change in sorbed water is observed. As the activity repeatedly scanned up and down between $a_w = 0.72$ and 0.92 (scans A/A′−G/G′), both $a_{w,e}$ and $a_{w,d}$ systematically increased (Figure 2). After the activity increased to $a_w = 0.95$ during scans G′ and H′, however, both $a_{w,e}$ and $a_{w,d}$ systematically decreased.

The coupling between the changes in $a_{w,e}$ and $a_{w,d}$ can be understood by considering the way the dissolution (deliquescence transition) during an upward scan depends on the population of lamellae that formed during crystallization (efflorescence transition) in the preceding downward scan. For example, the populations of lamellae that deliquesced during scans A′ and E′ were created during scans A ($a_{w,e} \approx 0.78$) and E ($a_{w,e} \approx 0.86$), respectively. Since lower $a_{w,e}$ results in a population of lamellae that is less stable, $a_{w,d}$ was smaller during scan A′ ($a_{w,d} \approx 0.89$) than during scan E′ ($a_{w,d} \approx 0.91$).

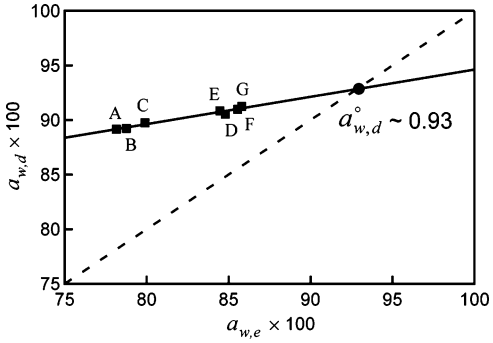

Figure 5. $a_{w,d}$ vs $a_{w,e}$ for seven consecutive scans (A/A′−G/G′) indicating a positive correlation between $a_{w,d}$ and the preceding $a_{w,e}$. A Hoffman−Weeks extrapolation estimates the equilibrium deliquescence activity of PEO ($a^\circ_{w,d} = 0.928$ at $T = 20.25$ °C), which describes the stability of the hypothetical infinite extended-chain crystal.

Throughout the sequence of scans between $a_w = 0.72$ and 0.92, $a_{w,d}$ increased linearly with increasing $a_{w,e}$ (Figure 5). This relationship between $a_{w,d}$ and $a_{w,e}$ is analogous to that observed between the crystallization temperature T_x and the melting temperature T_m during differential scanning calorimetry (DSC) experiments; lamellae grow thinner at deeper supersaturation (or subcooling) and, therefore, deliquesce (or melt) at more modest conditions. The equilibrium melting temperature T°_m of the hypothetical infinite extended-chain polymer crystal has been estimated by the intersection of the extrapolated linear dependence of T_m on T_x and the equilibrium line $T_m = T_x$; this analysis is known as the Hoffman−Weeks linear extrapolation.[1] Analogous extrapolation of the dependence of $a_{w,d}$ on $a_{w,e}$ yields an estimated equilibrium deliquescence activity $a^\circ_{w,d}$ of 0.928 (Figure 5). In light of recent criticisms of the classical Hoffman−Weeks extrapolation,[22,23] we recognize that this simple analysis likely underestimates $a^\circ_{w,d}$.

Another interesting coupling is observed in the efflorescence transition; the greater the water activity (i.e., the lower the supersaturation) at which the onset of crystallization occurs, the broader the efflorescence transition (Figure 4). Compare scans A′/B and E′/F, for example; in scan B, $a_{w,e}$ is lower and the transition is sharper than in scan F. Growth at higher a_w favors thicker lamellae, which may not fill space as densely as their thinner counterparts, since primary crystallization was not as complete during scan F as during scan B (Figure 4b). The gradual expulsion of water as a_w decreased from 0.85 to 0.72 during scan F suggests progressive enhancement of crystallinity, presumably resulting from secondary processes that were not required during scan B.

The response of PEO-2 to a programmed activity scan (at constant $T = 21.10 \pm 0.05$ °C) demonstrates gradual formation of a population of particularly stable lamellae over 12 h at constant activity in a partially dissolved state (Figure 6). Prior to this experiment, the PEO-2 solution droplet did not crystallize as a_w ramped down from 0.92 to 0.50 at 0.04 h^{-1}. The solution droplet was then rapidly quenched from $a_w = 0.50$ to $a_w = 0$ (still isothermal at $T = 21.10 \pm 0.05$ °C), causing it to crystallize (indicated by an abrupt change in the light scattering pattern). After 30 min at $a_w = 0$, the activity was stepped up to $a_w =$

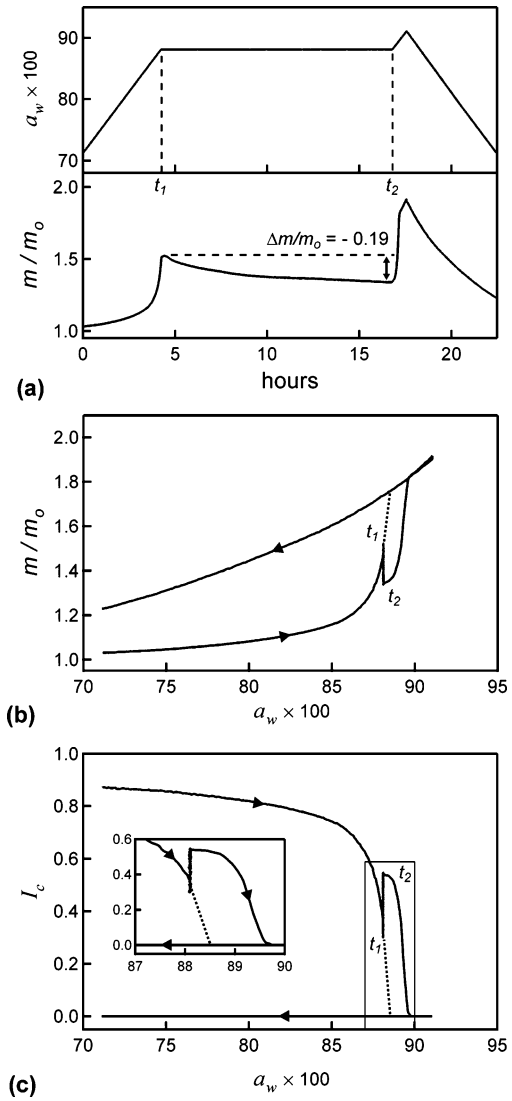

Figure 6. (a) Response of PEO-2 to a continuous triangular scan in water activity between 0.72 and 0.92 at 0.04 h^{-1} that paused at a_w = 0.88 for 12 h (from t_1 to t_2). (b) m/m_0 vs a_w and (c) I_c vs a_w indicate an increase in $a_{w,d}$ after the annealing time. $T = 21.10 \pm 0.05$ °C.

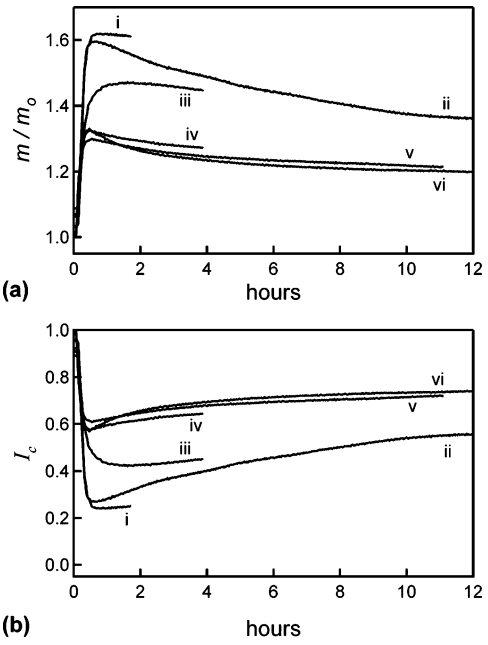

Figure 7. (a) m/m_0 and (b) I_c for PEO-3 in response to step changes from the dry semicrystalline state at $a_w = 0$ to the partially dissolved state at $a_w = 0.88$ (i, ii, and iii) and 0.87 (iv, v, and vi). $T = 21.10 \pm 0.05$ °C.

0.70 and held for 5 min to allow equilibration. The activity then ramped up from $a_w = 0.70$ to 0.88 at 0.04 h^{-1} and held at $a_w = 0.88$ for 12 h (t_1 to t_2 in Figure 6a) before continuing to increase to $a_w = 0.92$ at 0.04 h^{-1}. PEO-2 was partially dissolved at t_1, and the crystallinity slowly increased at constant $a_w = 0.88$, manifested by the gradual expulsion of water (m/m_0 had decreased by 0.19 at time t_2); this annealing step appears as a vertical decrease in mass in Figure 6b and a vertical increase in I_c in Figure 6c. As a_w then increased further, the remaining crystals dissolved to produce an aqueous solution droplet. The deliquescence after annealing, however, was shifted to greater a_w compared to the deliquescence that would have been observed without annealing (dotted line, Figure 6c inset).

The response of PEO-3 to step changes in activity from the dry to the partially dissolved state exhibits rapid dissolution of the lamellae that are not stable at the increased a_w (within ~30 min) followed by gradual formation of more stable lamellae (Figure 7). Duplicate experiments (trials i and ii) were annealed at $a_w = 0.88$ after crystallization during a quench to $a_w = 0$ (the particle was allowed to crystallize at $a_w = 0$ for 10 min). Trial iii was annealed at the same $a_w = 0.88$ after crystallization at a less severe supersaturation (a quench to $a_w = 0.70$ for 10 min). Since crystallization occurred at higher activity for trial iii, the sample contained a thicker population of lamellae and, therefore, initially dissolved to a lesser extent at $a_w = 0.88$ than did trials i and ii. Triplicate experiments (iv, v, and vi) were annealed at $a_w = 0.87$ after crystallization during a quench to $a_w = 0$ for 10 min. In all cases, the initial dissolution in response to the jump in water activity was rapid. For samples that have the same solid state history, the fraction of the lamellar population that rapidly dissolved is greater for a jump to $a_w = 0.88$ (i and ii) than a jump to $a_w = 0.87$ (iv, v, and vi). For samples jumped to the same elevated activity, the fraction that rapidly dissolved is greater for those crystallized rapidly at a deep supersaturation (i and ii) than those crystallized slowly at a mild supersaturation (iii). In all cases, subsequent increase in crystallinity was very slow.

Discussion

Our interpretation of these results is organized as follows. First, the above observations indicate that crystalline remnants after dissolution of the solid state persist at activities substantially beyond that which dissolves all detectable lamellae. Analogous to memory effects observed in the melt, these remnants persist beyond the observed deliquescence activity, just as the melt memory effect persists beyond the nominal melting temperature. Second, we argue that the strong asymmetry in kinetics between lateral growth or dissolution and lamellar thickening governs the dissolution trajectory of a lamella and, hence, the geometry of the remnant it may leave behind. Finally, we offer an integrated thermodynamic/kinetic perspective that is capable of describing the existence and evolution of athermal nuclei. In accord with the ideas of Janeschitz-Kriegl,[16−18] we show that a model of interfacial energy of the fold surface that reflects the reduced constraints near the perimeter of a lamella captures the observed behavior, which, in contrast, the conventional treatment of the surface energy of fold surface as uniform does not.

Existence and Persistence of Crystal Remnants. Systematic manipulation of $a_{w,e}$ (Figure 2) indicates that crystallization that

occurred during these efflorescence events in aqueous PEO is not initiated by homogeneous thermal nucleation, which would exhibit random variation about some average $a_{w,e}$ with repeated experiments.[20] We believe instead that crystallization is catalyzed by persistent remnants of dissolved lamellae, which serve as athermal nuclei. If these remnants are clusters containing a small number of molecular segments and folds, the cluster length would correlate with the conditions at which a cluster initiates lateral crystal growth; i.e., clusters of decreasing length should require a greater supersaturation to become "awake". Consequently, the systematic increase (or decrease) in $a_{w,e}$ during repeated scans to $a_w = 0.92$ (or 0.95) indicates that the population of athermal nuclei in solution shifts to increased (or decreased) length in response to certain processing histories.

These clusters must be sufficiently small that they do not affect Mie scattering, so they are submicron sized. They can also persist for hours while the humidity is above the value that causes lamellar crystals to dissolve ($a_{w,d}$). In Figure 2, for example, the elapsed time from the completion of deliquescence to the time that a_w returns to that value during the subsequent downward scan is ~2 h. These clusters must, therefore, have an exemption from the physics that drives chains to dissolve from edges of large lamellae since, following a sudden jump up to $a_w = 0.88$, the dissolution of lamellae that are unstable at this condition is complete in less than 30 min (Figure 7). The persistence and evolution of the remnants, therefore, cannot be attributed exclusively to sluggish dissolution kinetics; thermodynamic considerations are required to rationalize their long lifetime.

Kinetic Considerations in Formation of Crystal Remnants. In accord with prior literature, the results above show that the rate at which lamellae increase in radius during efflorescence (Figures 3 and 4) is significantly greater than the rate of lamellar thickening (Figures 6 and 7).[3,4] Although it is not possible to quantify the rate of thickening during prolonged annealing at a partially deliquesced state, we can confirm that thickening has occurred from the shape of the subsequent deliquescence (Figure 6). In the inset of Figure 6c it is clear that I_c remains nearly constant when a_w is increased from the value at which it was annealed (0.880) to the value at which the index would have vanished (0.885) if the rame in water activity had been continued without interruption (dotted line). Thus, all of the lamellae that were present at time t_1 must have dissolved or thickened during the annealing time. The increase in T_c during annealing did not occur by lateral growth at fixed thickness of those lamellae that remained at time t_1, nor did I_c increase simply by adding a population of thicker lamellae to those suriviving at time t_1. Based on the character of the free energy surface discussed below, we infer that the dominant mechanism of increase in I_c is thickening. The free energy is a very steep function of thickness, so the cutoff between those lamellae that dissolve early during the annealing period and those that survive indefinitely at $a_{w,anneal}$ is very sharp. Therefore, the long-time process has negligible contribution from "borderline" lamellae of thicknesses that would require hours to dissolve.

Integrated Thermodynamic/Kinetic Perspective. As a point of departure for modeling the free energy of small clusters, consider classical nucleation theory for a droplet of pure liquid nucleating from a supersaturated vapor.[24,25] The change in free energy of the system upon formation of a condensed cluster is approximated as the energy decrease due to the difference in free energy per unit volume Δf between the stable and metastable phases offset by an energy increase that depends on the size of the cluster (usually attributed to the formation of an

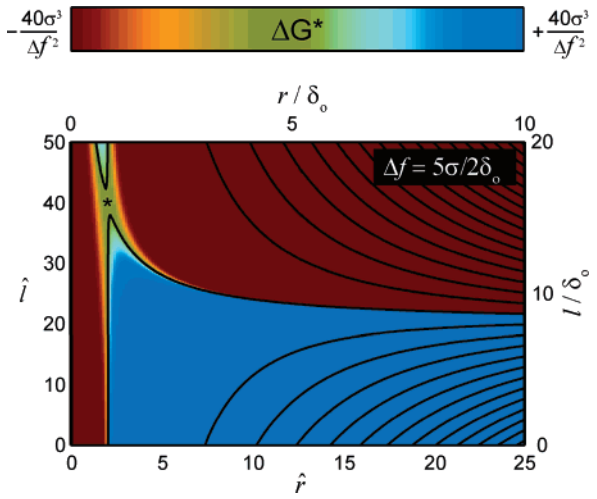

Figure 8. Contour map of ΔG (eq 3) with $\alpha_e = 10$, and $\Delta\mu = 5v_m\sigma/2\delta_0$. Bottom and left axes are normalized by the characteristic length scale $\sigma v_m/\Delta\mu$. Top and right axes are normalized by a constant length δ_0. The asterisk marks the saddle point. Contour lines are equally spaced in energy. Regions with much lower free energy than the saddle point are red; the region with much greater free energy than the saddle point is blue. In the vicinity of the saddle point, variations in free energy are indicated by a highly magnified color sacle (the entire range of the color shown at the top is approximately 2% of the free energy increment between contour lines).

interface with surface tension σ). The natural length scale $\sigma/\Delta f$ dictates the critical nucleus size that distinguishes growing from decaying clusters.

Although the classical nucleation picture may be oversimplified, the qualitative features of its free energy landscape are instructive, particularly when applied to platelet-like volumes of crystal formed from solution. Regarding chain-folded crystals of polymers, this simple picture is extended to allow the fold surface to have a different tension σ_e than that of the lateral surfaces, σ; experimental evidence suggests that σ_e is much greater than σ (by as much as a factor of 10).[1] Considering a disk-shaped polymer crystal of radius r and thickness l, the free energy of formation of a lamella from an amorphous melt or solution is then modeled as

$$\Delta G(r,l) = -\pi r^2 l\Delta f + 2\pi r l\sigma + 2\pi r^2\sigma_e \qquad (2)$$

In nondimensional form this becomes

$$\Delta G(\hat{r}, \hat{l})\frac{\Delta f^2}{\pi\sigma^3} = -\hat{r}^2\hat{l} + 2\hat{r}\hat{l} + 2\alpha_e\hat{r}^2 \qquad (3)$$

where $r = \hat{r}\sigma/\Delta f$, $l = \hat{l}\sigma/\Delta f$, and $\sigma_e = \alpha_e\sigma$. Here we consider $\Delta f > 0$; i.e., the sample is below the equilibrium melting temperature or the equilibrium deliquescence solvent activity. As we discuss the relationship between the free energy surface and the growth or dissolution of lamellae, we note again that lamellae are kinetically prevented from evolving strictly along contours of steepest descent because the thickening process of a lamella is very slow compared to the rate that segments can add or detach from the lateral faces of the lamella. It is, therefore, reasonable to assume that in response to a step decrease in Δf an unstable lamella of size (r_0, l_0) will rapidly decrease in radius; i.e., the crystallite will either vanish or quickly reach a metastable radius, if one exists for $l = l_0$.

To see that this conventional treatment (fold surface of uniform energy) does not permit the persistence of small crystalline clusters, consider the fate of initially very wide lamellae following the step decrease in Δf. As is usually the

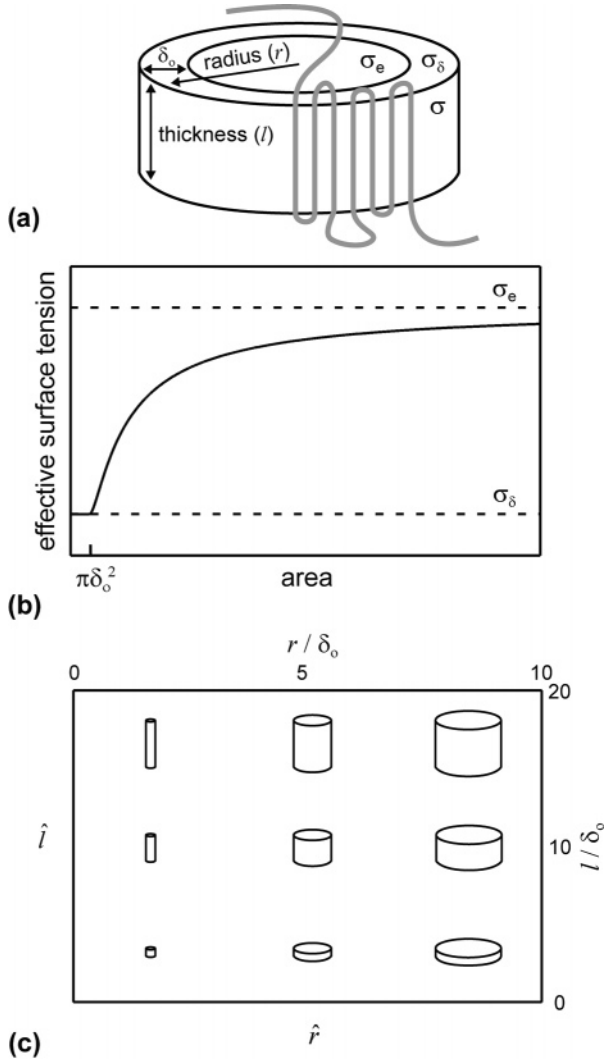

Figure 9. (a) Schematic of a disk-shaped lamellar crystal of thickness l and radius r and three distinct surface tensions (σ, σ_e, and σ_δ). An annulus of width δ_0 defines the low energy perimeter of the fold surface. (b) Average surface tension of the fold surface as a function of the fold surface area. (c) Schematic indicating the aspect ratio of lamellar crystals in various regions of the contour maps of Figures 8 and 10. The diagonal represents crystals with $l = 2r$.

case for semicrystalline polymers, finite thickness lamellae are metastable and could proceed downhill in free energy if they could thicken; i.e., $\partial\Delta G/\partial\hat{l}$ is negative for sufficiently wide lamellae ($\hat{r} > 2$):

$$\frac{\partial\Delta G}{\partial\hat{l}}\frac{\Delta f^2}{\pi\sigma^3} = -\hat{r}^2 + 2\hat{r} = 0 \quad \text{for} \quad \hat{r} = 2 \tag{4}$$

However, given the kinetic obstacle to changes in thickness, the lamellae initially only respond to the gradient in free energy with respect to radius. For sufficiently thick lamellae ($\hat{l} > 2\alpha_e$, e.g., $\hat{l} > 20$ in Figure 8), the free energy generally decreases with increasing radius, i.e., $\partial\Delta G/\partial\hat{r} < 0$ for large $\hat{r}$. Thin lamellae ($\hat{l} < 2\alpha_e$), on the other hand, move monotonically downhill in free energy by decreasing in radius:

$$\frac{\partial\Delta G}{\partial\hat{r}}\frac{\Delta f^2}{\pi\sigma^3} = -2\hat{r}\hat{l} + 2\hat{l} + 4\alpha_e\hat{r} > 0 \quad \text{for} \quad \hat{l} < \frac{2\alpha_e\hat{r}}{\hat{r}-1} \text{ and } \hat{r} > 1 \tag{5}$$

For comparison with the alternative model below, note that there is a saddle point in the free energy surface at $(\hat{r}^*, \hat{l}^*) = (2, 4\alpha_e)$, but there are no local minima with respect to change in radius (Figure 8). The points at which $\partial\Delta G/\partial\hat{r} = 0$, $\hat{l} = 2\alpha_e\hat{r}/(\hat{r} - 1)$ according to eq 5, represent local maxima with respect to changes in radius, as indicated by eq 6.

$$\left.\frac{\partial^2\Delta G}{\partial\hat{r}^2}\right|_{\partial\Delta G/\partial\hat{r}=0} = 4\alpha_e\left(\frac{1}{1-\hat{r}}\right) < 0 \quad \text{for} \quad \hat{r} > 1 \tag{6}$$

Thus, this model cannot explain the persistence of small lamellar remnants; all lamella that would decay in radius decay monotonically until they vanish.

Janeschitz-Kriegl convincingly argues that dangling ends and folds experience greater conformational freedom along the edge of the fold surface than in the crowded interior. He suggests that the effective surface tension σ_e, therefore, increases sigmoidally as the fold surface area increases.[18] A simple way to capture the essence of this J−K model is to divide the fold surface into a core region with high surface tension $\sigma_e = \alpha_e\sigma$ and an annulus of width δ_0 along its perimeter with lower surface tension $\sigma_\delta = \alpha_\delta\sigma$ ($\alpha_\delta \approx 1$),[16] as depicted in Figure 9.

The free energy of formation of such a lamellar disk can be expressed in nondimensional form as

$$\Delta G_{J-K}(\hat{r}, \hat{l})\frac{\Delta f^2}{\pi\sigma^3} = \begin{cases} -\hat{r}^2\hat{l} + 2\hat{r}\hat{l} + 2\alpha_e(\hat{r} - \hat{\delta}_0)^2 + 2\alpha_\delta(\hat{r}^2 - (\hat{r} - \hat{\delta}_0)^2) & \hat{r} > \hat{\delta}_0 \\ -\hat{r}^2\hat{l} + 2\hat{r}\hat{l} + 2\alpha_\delta\hat{r}^2 & \hat{r} \le \hat{\delta}_0 \end{cases} \tag{7}$$

where $\delta_0 = \hat{\delta}_0\sigma/\Delta f$. Examining the first partial derivatives for local extrema reveals that

$$\frac{\partial\Delta G_{J-K}}{\partial\hat{l}}\frac{\Delta f^2}{\pi\sigma^3} = 0 \quad \text{for } \hat{r} = 2 \tag{8}$$

and

$$\frac{\partial\Delta G_{J-K}}{\partial\hat{r}}\frac{\Delta f^2}{\pi\sigma^3} = 0 \quad \text{for} \quad \hat{l} = \begin{cases} \dfrac{2\alpha_e\hat{r} - 2\hat{\delta}_0(\alpha_e - \alpha_\delta)}{\hat{r} - 1} & \hat{r} > \hat{\delta}_0 \\ \dfrac{2\alpha_\delta\hat{r}}{\hat{r} - 1} & \hat{r} \le \hat{\delta}_0 \end{cases} \tag{9}$$

In contrast to the classical model presented above, the saddle point $(\hat{r}^*, \hat{l}^*) = (2, 4\alpha_e - 2\hat{\delta}_0(\alpha_e - \alpha_\delta))$ in this free energy surface is accessible to radially shrinking lamellae under thermodynamic conditions such that $\hat{l}^*$ is less than the marginal thickness at which very wide lamellae decay (red/blue transition in Figure 10). Furthermore, these conditions enable the free energy surface to trap small remnants since local free energy minima with respect to changing radius exist in the vicinity of the saddle point (Figure 11a). These conditions are satisfied when

$$2 > \hat{\delta}_0 = \frac{\delta_0\Delta f}{\sigma} > \frac{\alpha_e}{\alpha_e - \alpha_\delta} \tag{10}$$

In this case, a wide and sufficiently thin lamella ($\hat{l} < 2\alpha_e$) will rapidly decrease in radius until it reaches the valley in the free energy landscape near the saddle point and then slowly change in thickness toward a lower energy state.

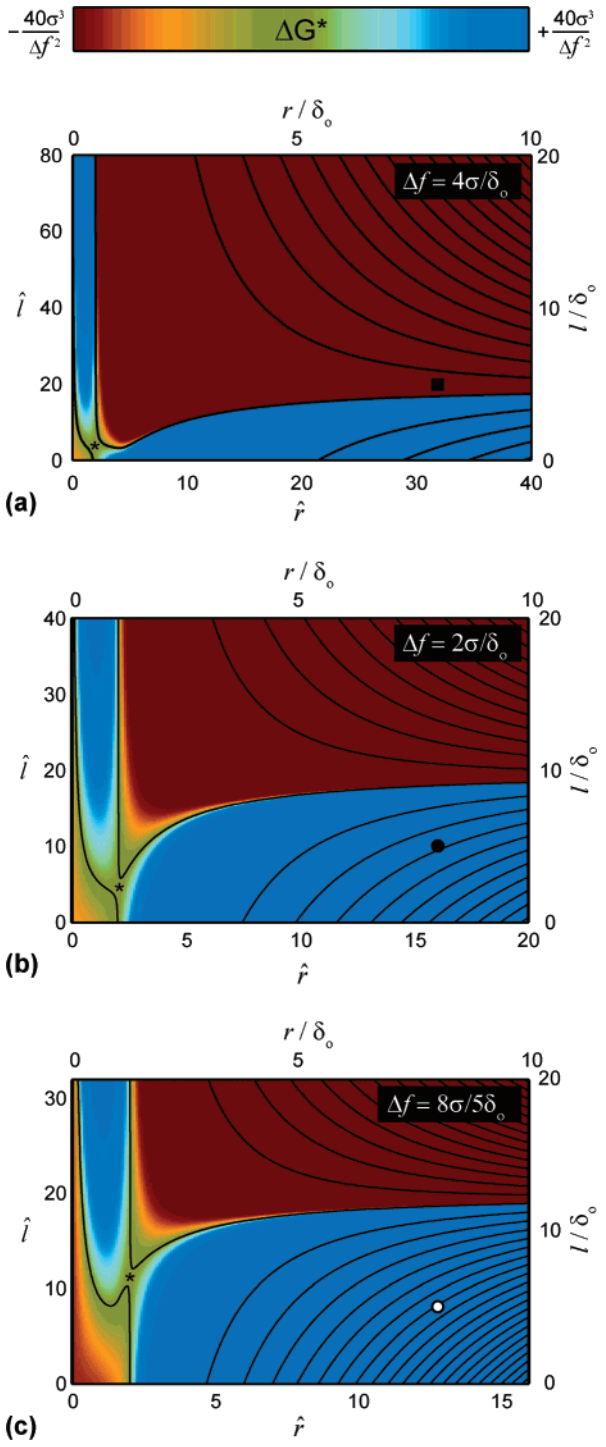

Figure 10. Contour maps of ΔG_{J-K} (eq 7) with $\alpha_\delta = 1$, $\alpha_e = 10$, and (a) $\Delta\mu = 4v_m\sigma/\delta_0$, (b) $\Delta\mu = 2v_m\sigma/\delta_0$, and (c) $\Delta\mu = 8v_m\sigma/5\delta_0$. Bottom and left axes are normalized by the characteristic length scale $\sigma v_m/\Delta\mu$. Top and right axes are normalized by a constant length δ_0. The symbols ■, ●, and ○ indicate identical lamellae with $r = 8/\delta_0$ and $l = 5/\delta_0$. See caption of Figure 8 for explanation of color scale.

As the depth of metastability, Δf, decreases (corresponding to increasing a_w or temperature), we observe two expected trends in the J−K free energy landscape in the progression from Figure 10a to 10c: (i) the stability of crystals of a given thickness decreases (i.e., the blue region extends to greater l/δ_0 as Δf decreases), and (ii) the saddle point shifts to greater thickness (i.e., the lowest energy path to formation of a stable crystalline entity from the melt or solution requires greater crystal thickness). We also notice changes in the detailed shape of the saddle with decreasing Δf, which affects how trapped clusters evolve in thickness. When $\Delta f = 4\sigma/\delta_0$ or $\Delta f = 2\sigma/\delta_0$ (Figure 10a,b), a local minimum with respect to changes in radius only occurs for lamellar thicknesses that are greater than the saddle point value ($\hat{l} > \hat{l}^*$); i.e., the lamellar remnants that can be trapped in the free energy landscape of Figure 10a,b already start with sufficient thickness that they will thicken further. On the other hand, when $\Delta f = 8\sigma/5\delta_0$ (Figure 10c), a local minimum with respect to changes in radius also exists for some values of $\hat{l} < \hat{l}^*$. Thus, in the landscape of Figure 10c, the thickness of trapped clusters may increase or decrease, depending on the initial thickness of the lamella that is dissolving.

To illustrate the dynamics of lamellae under various conditions, consider a lamella with thickness $l = 5\delta_0$ and radius $r = 8\delta_0$ on each of the three free energy surfaces of Figure 10 (indicated by ■, ●, and ○ in Figure 11a). As discussed previously, the kinetics of changing radius are much faster than the kinetics of changing thickness, and so the initial trajectory of the lamella can be reasonably estimated by examining a sectional view of the surface at fixed $l = 5\delta_0$ (Figure 11a). For the deepest supersaturation, $\Delta f = 4\sigma/\delta_0$ (A in Figure 11a), the lamella grows radially, but a lamella of this thickness dissolves at the two shallower supersaturations, $\Delta f = 2\sigma/\delta_0$ and $\Delta f = 8\sigma/5\delta_0$ (B and C in Figure 11a), and its radius decreases until it reaches a local free energy minimum. The coordinate of the trapped cluster in each case has been indicated on an expanded view of the free energy saddle for conditions B and C (Figure 11b,c). Cluster B has a thickness $\hat{l} > \hat{l}^*$ and reduces its free energy by slowly evolving toward increased thickness and radius. Cluster C has a thickness $\hat{l} < \hat{l}^*$ and reduces its free energy by slowly evolving toward decreased thickness and radius.

To map a correspondence between the J−K free energy model presented above and the experimental conditions for the PEO/water system, we consider the reported bulk enthalpy of formation of PEO crystallites from the melt, ΔH_f, the equilibrium melting point, T_m°, and, additionally, the thermodynamics of aqueous PEO solution. Usually the reference state for the bulk free energy of crystallites is the melt, and the change in free energy upon transformation of molten chains into a hypothetical infinite crystal per unit volume of crystal is approximated by[1]

$$\Delta f_{m-c} = f_{melt} = f_{crystal} \approx \frac{\Delta H_f(T_m^\circ - T)}{T_m^\circ} \tag{11}$$

Here, we must also account for the change in free energy of a polymer chain between the melt and the solvated state.

$$\Delta f = f_{solution} - f_{crystal} = \Delta f_{s-m} + f_{m-c} \tag{12}$$

In a typical polymer solution with nonspecific polymer/solvent interactions, the Flory−Huggins theory provides a model for the chemical potential of the polymer

$$\Delta\mu_p = \Delta f_{s-m} v_p \rho_p \tag{13}$$

where v_p is the molar volume and ρ_p is the density of the polymer.[27] This approach does not, however, accurately describe the aqueous PEO system because of the unique solubility of PEO in water.[28] Nevertheless, the Gibbs−Duhem relationship remains valid

$$n_w\, d\mu_w + n_p\, d\mu_p = 0 \tag{14}$$

where subscripts w and p denote water and polymer, n_i is the number of moles of species i, and μ_i is the chemical potential.

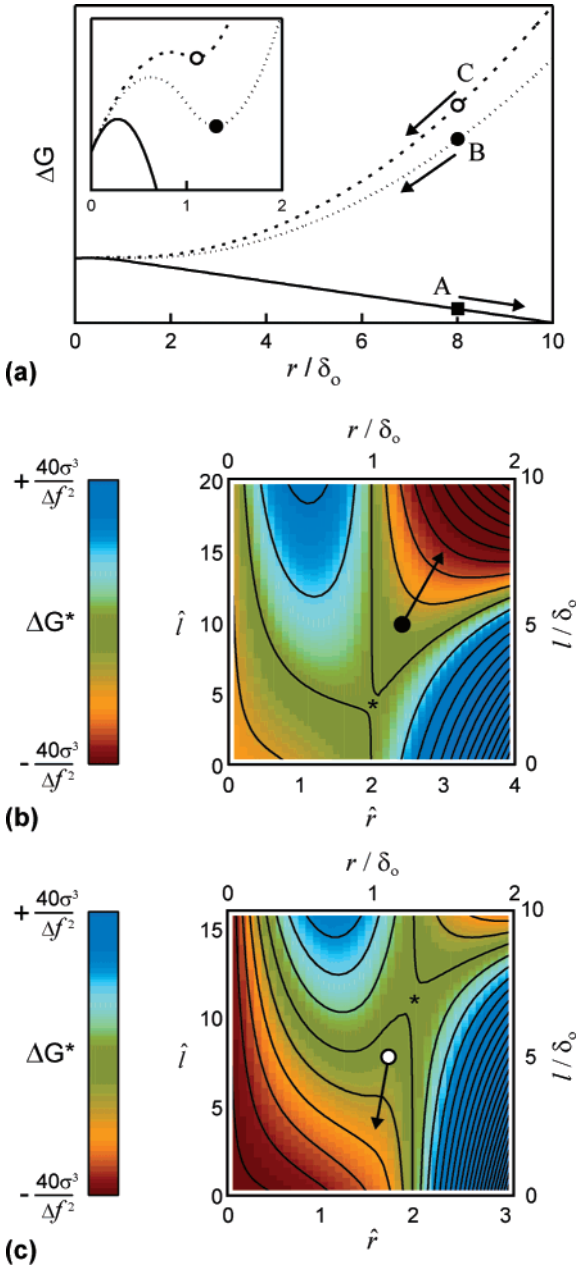

Figure 11. (a) ΔG_{J-K} as a function of radius for constant $l = 5\delta_0$ for the conditions of Figures 10a (A, ■), 10b (B, ●), and 10c (C, ○). The inset depicts an expanded view at small radius, revealing local minima that trap clusters B and C at finite radius. Also, expanded views of the saddles in (b) Figure 10b and (c) Figure 10c that trap a cluster under conditions in which they reduces their free energy by (b) increasing and (c) decreasing in thickness.

In other words, a differential change in the imposed activity of water, and hence its chemical potential, $\mu_w = RT \ln a_w$, is accompanied by an offsetting change in the chemical potential of the polymer. For example, an increase in water activity ($d\mu_w > 0$) must occur with a decrease in the chemical potential of the polymer ($d\mu_p < 0$); therefore, the polymer must become more dilute by uptake of water (increase in n_w at fixed n_p in the levitated solution droplet). The chemical potential of polymer at an arbitrary chemical potential of water can thus be calculated by integrating eq 14 from the dry molten state to the aqueous solution at specified μ_w

$$\Delta\mu_p(\mu_w) = \mu_{p,sol}(\mu_w) - \mu_{p,melt} = -\int_{melt}^{\mu_w} \frac{n_w(\mu_w')}{n_p} d\mu_w' \quad (15)$$

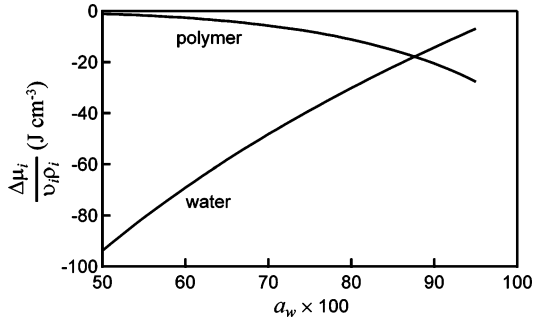

Figure 12. Difference in free energy per unit volume of the polymer and of water between the solution and the pure state as a function of water activity. The water trace was calculated from the imposed water activity ($\mu_w = RT \ln a_w$). The polymer trace was computed numerically according to eq 15.

Table 1. Thermodynamic Parameters Relating J−K Model to Experimental Conditions

Δf	σ [erg/cm²]	δ_0 [nm]	$\Delta f_{m-c} + \Delta f_{s-m}$ [J/cm³]	Δf_{m-c} [J/cm³]	Δf_{s-m} [J/cm³]	a_w (est)
$4\sigma/\delta_0$	10	1	40	43	−3	0.616
$2\sigma/\delta_0$	10	1	20	43	−23	0.919
$8\sigma/5\delta_0$	10	1	16	43	−27	0.945

using the measured water uptake n_w as a function of μ_w. We compute the integral numerically using data measured between $a_w = 0.75$ and 0.93 and an approximate fit[29] for $a_w < 0.75$ (Figure 12).

Using eq 11 and literature values of $\Delta H_f = 266$ J/cm³ and $T_m^\circ = 77$ °C,[26] Δf_{m-c} is estimated as 43 J/cm³ at 20 °C. Using eq 12, this Δf_{m-c}, and values of $\Delta f_{s-m} = \Delta\mu_p/\upsilon_p\rho_p$ from Figure 12, $\Delta f = \Delta f_{m-c} + \Delta f_{s-m}$ is estimated as a function of a_w. After selecting reasonable values for σ (10 erg/cm²) and δ_0 (1 nm), the thermodynamic conditions represented in Figure 10 can be correlated with experimental values of a_w. The analysis suggests that the free energy maps in Figure 10 represent thermodynamic conditions that are readily accessible by SAGA (Table 1): $a_w = 0.616$ ($\Delta f = 4\sigma/\delta_0$) represents growth conditions, $a_w = 0.919$ ($\Delta f = 2\sigma/\delta_0$) represents dissolution conditions under which remnants will increase in thickness, and $a_w = 0.945$ ($\Delta f = 8\sigma/5\delta_0$) represents dissolution conditions under which remnants will decrease in thickness.

Extension of SAGA to General Polymer/Solvent Systems. In the current work, PEO crystals deliquesce in a humid environment near ambient temperature because of their water solubility and their relatively low melting point (nominally 65 °C), i.e., Δf_{m-c} is sufficiently small at ambient temperature that lamellar crystals can be destabilized by sorption of solvent into the interlamellar non-crystalline material. The analysis presented above predicts that the deliquescence activity of a given sample will decrease with increasing temperature. (We have confirmed this experimentally, although over a modest range of just a few kelvin due to instrument limitations.) SAGA may thus be extended to the study of phase transitions in other semicrystalline polymers by developing the capability to create a controlled atmosphere of arbitrary solvent vapor at arbitrary temperature.

Acknowledgment. The authors dedicate this paper to Hermann Janeschitz-Kriegl on the occasion of his 82nd birthday and thank him for stimulating this work. The authors also thank Zhen-Gang Wang of the California Institute of Technology for insightful discussions. This material is based upon work supported by the National Science Foundation under Grants 0505393 and 0080065.

CDV

References and Notes

(1) Hoffman, J. D.; Davis, G. T.; Lauritzen, J. I., Jr. The rate of crystallization of linear polymers with chain folding. In *Treatise on Solid-State Chemistry*; Hannay, N. B., Ed.; Plenum: New York, 1976; Vol. 3, Chapter 7.
(2) Verma, R.; Marand, H.; Hsiao, B. *Macromolecules* **1996**, *29*, 7767.
(3) Marand, H.; Huang, Z. *Macromolecules* **2004**, *37*, 6492.
(4) Abo el Maaty, M. I.; Bassett, D. C. *Polymer* **2005**, *46*, 8682.
(5) Blundell, D. J.; Keller, A.; Kovacs, A. J. *Polym. Lett.* **1996**, *4*, 487.
(6) Fillon, B.; Wittman, J. C.; Lotz, B.; Thierry, A. *J. Polym. Sci.* **1993**, *31*, 1383.
(7) Feng, Y.; Jin, X. *J. Appl. Polym. Sci.* **1999**, *72*, 1559.
(8) Massa, M. V.; Lee, M. S. M.; Dalnoki-Veress, K. *J. Polym. Sci., Part B: Polym. Phys.* **2005**, *43*, 3438.
(9) Alfonso, G. C.; Ziabicki, A. *Colloid Polym. Sci.* **1995**, *273*, 317.
(10) Alfonso, G. C.; Scardigli, P. *Macromol. Symp.* **1997**, *118*, 323.
(11) Lehnert, R. J.; Hirschmann, H. *Polym. J.* **1997**, *29*, 100.
(12) Sasaki, T.; Yamamoto, Y.; Takahashi, T. *Polym. J.* **2000**, *32*, 263.
(13) Häfele, A.; Heck, B.; Hippler, T.; Kawai, T.; Kohn, P.; Strobl, G. *Eur. Phys. J. E* **2005**, *16*, 217.
(14) Fischer, J. C.; Hollman, J. H.; Turnbull, D. *J. Appl. Phys.* **1948**, *19*, 775.
(15) Ziabicki, A.; Alfonso, G. C. *Colloid Polym. Sci.* **1994**, *272*, 1027.
(16) Janeschitz-Kriegl, H. *Colloid Polym. Sci.* **1997**, *275*, 1121.
(17) Janeschitz-Kriegl, H.; Ratajski, E.; Wippel, H. *Colloid Polym. Sci.* **1999**, *277*, 217.
(18) Janeschitz-Kriegl, H. *Colloid Polym. Sci.* **2003**, *281*, 1157.
(19) Olsen, A. P.; Flagan, R. C.; Kornfield, J. A. *Macromolecules* **2006**, *39*, 5946.
(20) Olsen, A. P.; Flagan, R. C.; Kornfield, J. A. *Rev. Sci. Instrum.* **2006**, *77*, 073901.
(21) van de Hulst, H. C. *Light Scattering by Small Particles*; Wiley: New York, 1957.
(22) Marand, H.; Xu, J.; Srinivas, S. *Macromolecules* **1998**, *31*, 8219.
(23) Strobl, G. *Prog. Polym. Sci.* **2006**, *31*, 398−442.
(24) Becker, R.; Döring, W. *Ann. Phys.* **1935**, *24*, 719.
(25) Seinfeld, J. H.; Pandis, S. N. *Atmospheric Chemistry and Physics*; Wiley: New York, 1998.
(26) Schönherr, H.; Frank, C. *Macromolecules* **2003**, *36*, 1199.
(27) Rigorous treatment of differences in polymer density between the melt, solution, and crystal have been omitted for simplicity.
(28) Fischer, V.; Borchard, W.; Karas, M. *J. Phys. Chem.* **1996**, *100*, 15992.
(29) For $a_w < 0.75$, for which data were not available, the sorbed water content was empirically approximated by a fifth-order power law: $n_w/n_p = Aa_w^5$ (A = constant), such that the value and slope match the experimental data at $a_w = 0.75$.

MA0614949